Advances in Applied Mathematics and Mechanics
Adv. Appl. Math. Mech., Vol. **7**, No. 3, pp. 295-322

DOI: 10.4208/aamm.2014.m544
June 2015

An Efficient Semi-Analytical Method to Compute Displacements and Stresses in an Elastic Half-Space with a Hemispherical Pit

Valeria Boccardo[1,2], Eduardo Godoy[3,*] and Mario Durán[1]

[1] *Facultad de Ingeniería, Pontificia Universidad Católica de Chile, Av. Vicuña Mackenna 4860, Macul, Santiago, Chile*
[2] *Facultad de Ingeniería, Universidad Mayor, Av. Manuel Montt 367, Providencia, Santiago, Chile*
[3] *Ingenieros Matemáticos Consultores Asociados S.A. (INGMAT), José Miguel de la Barra 412, 4to piso, Santiago, Chile*

Received 19 March 2014; Accepted (in revised version) 3 October 2014

Abstract. This paper presents an efficient method to calculate the displacement and stress fields in an isotropic elastic half-space having a hemispherical pit and being subject to gravity. The method is semi-analytical and takes advantage of the axisymmetry of the problem. The Boussinesq potentials are used to obtain an analytical solution in series form, which satisfies the equilibrium equations of elastostatics, traction-free boundary conditions on the infinite plane surface and decaying conditions at infinity. The boundary conditions on the free surface of the pit are then imposed numerically, by minimising a quadratic functional of surface elastic energy. The minimisation yields a symmetric and positive definite linear system of equations for the coefficients of the series, whose particular block structure allows its solution in an efficient and robust way. The convergence of the series is verified and the obtained semi-analytical solution is then evaluated, providing numerical results. The method is validated by comparing the semi-analytical solution with the numerical results obtained using a commercial finite element software.

AMS subject classifications: 35Q74, 35C10, 74G15

Key words: Elastic half-space, semi-infinite domain, axisymmetric domain, hemispherical pit, semi-analytical solution.

*Corresponding author.
Email: vhboccar@puc.cl (V. Boccardo), eduardo.godoy@ingmat.com (E. Godoy), mduran@ing.puc.cl (M. Durán)

 ©2015 Global Science Press

https://doi.org/10.4208/aamm.2014.m544 Published online by Cambridge University Press

1 Introduction

Boundary-value problems of linear elastostatics in unbounded domains are of current interest in various disciplines related to earth sciences, such as geophysics, soil and rock mechanics, structural and foundation engineering, and mining engineering, among others. To determine stresses and displacements around certain structures of interest such as tunnels, cracks, or underground and open-pit excavations, it is necessary, in order to produce accurate results, to take into account the surrounding medium, which for modelling purposes is assumed to be an unbounded elastic domain. In particular, the main motivation of the present investigation comes from the need for calculating the stresses and displacements induced by gravity in a mining excavation, in order to determine the areas in risk of collapse due to high-stress concentration. For this, the surrounding rock mass needs to be taken into account.

To define a methodology for solving this type of problems, the unboundedness of the domain represents a major difficulty. Numerical methods appear to be a good alternative to solve boundary-value problems in general, however, most of them require a bounded computational domain. This problem is often solved by truncating artificially the unbounded domain, reducing the original problem to a bounded domain. Nevertheless, artificial boundary conditions have to be imposed on its boundary in order to obtain correct results. The choice of such boundary conditions is not clear a priori, constituting this issue in itself a whole area of research. Another alternative is to calculate an analytical solution to the unbounded boundary-value problem. Even though it is well-known that analytical solutions have the disadvantage of being possible only for certain simple geometries, they are useful since they can be used to deduce artificial boundary conditions for a truncated domain, which is then discretized numerically. Some authors who have followed this approach in linear elastostatics are Han and Wu [13, 14], Givoli and Keller [9], and Givoli and Vigdergauz [10].

Most of the analytical solutions for unbounded elastic domains available in the literature are for exterior domains with simple geometries. In particular, the solutions provided in [9,13,14] are for the exterior of a circle. Even though these analytical solutions may be used in applications related to geosciences, a more precise approximation of the unbounded medium that surrounds an excavation (or another similar structure) is achieved with a half-plane or a half-space, with the excavation represented as a local perturbation. This type of domain is called semi-infinite and has the difficulty of being bounded by an infinite plane surface, which is assumed to be traction-free in most cases. Nevertheless, analytical solutions are still possible for some simple geometries. In the two-dimensional case, certain complex variable methods have proven to be useful for that purpose. Givoli and Vigdergauz [10] employed Kolosoff-Muskhelishvili potentials to solve the elastostatic problem at the exterior of a semicircle in a half-plane and used the obtained solution to derive artificial boundary conditions for geophysical applications. A similar technique was applied by Verruijt [18, 19] to solve the problem of an elastic half-plane with an embedded circular cavity.

https://doi.org/10.4208/aamm.2014.m544 Published online by Cambridge University Press

In the case of three-dimensional semi-infinite domains, a number of efforts have been made in order to solve analytically the problem of a hemispherical pit in the surface of an elastic half-space. The first work on this regard was done by Eubanks [6], who derived expressions for the axisymmetric stresses and displacements around the pit in series form. Some generalisations of his results were provided by Fujita et al. for the cases where the domain is an unbounded thick plate instead of a half-space [7], and where the stress and displacement fields are no longer axisymmetric but asymmetric [8]. Eubanks employs the so-called Boussinesq potentials to obtain an analytical solution as infinite series satisfying traction-free boundary conditions on the plane surface and decaying conditions at infinity. However, imposing boundary conditions on the surface of the pit leads to an infinite set of simultaneous linear equations for the coefficients of the series, which cannot be solved exactly. After some unwieldy algebraic manipulation, these equations are solved numerically, yielding approximate values for a finite number of coefficients. Hence, the solution given in [6] is actually not fully analytical but semi-analytical, and similar phenomena occur in [7, 8, 10, 18, 19]. In addition, the numerical evaluation of the solution in [6] involves computing the sum of double series that show a slow convergence at the surface of the pit, which is computationally expensive and further complicates obtaining explicitly the solution.

This paper is concerned with solving the problem of a hemispherical pit on the surface an elastic half-space, assumed to be in equilibrium under its own weight. The displacement and stress fields around the pit are sought in axisymmetric form, taking advantage of the axisymmetry of the problem. The procedure to calculate the solution is to a certain extent based upon the one made by Eubanks [6], but the proposed analytical solution is improved by including an additional term in the series of one of the Boussinesq potentials, which, to the authors' opinion, needs to be considered in the analysis. Furthermore, the boundary conditions on the hemispherical pit are herein imposed by minimising a quadratic functional representing the surface elastic energy. Even though this approach does not eliminate the problem of an infinite number of equations and coefficients, it provides a systematic method to deal with it. The minimisation of the functional leads to a linear system of equations for a finite number of coefficients of the series. The associated matrix is symmetric, positive definite and possesses a particular block structure that allows us to solve it in an efficient and robust way, thus avoiding to have to deal with cumbersome equations and slowly convergent double series.

2 Mathematical formulation

In this section, the mathematical model describing the elastic deformations and stresses in a half-space with a hemispherical pit is formulated. For this purpose, we first consider the half-space without the pit, occupied by an isotropic linear elastic solid of density ρ representing the rock mass. We deal with the lower half-space, denoted by $\mathbb{R}^3_-$, which is defined in cartesian coordinates x, y, z as $\mathbb{R}^3_- = \{(x,y,z) \in \mathbb{R}^3 : z < 0\}$. Let us denote

https://doi.org/10.4208/aamm.2014.m544 Published online by Cambridge University Press

by $\boldsymbol{u}:\mathbb{R}^3_- \to \mathbb{R}^3$ a generic displacement field. The stress tensor, denoted by $\boldsymbol{\sigma}$, is given in terms of $\boldsymbol{u}$ by the isotropic Hooke's law, that is,

$$\boldsymbol{\sigma}(\boldsymbol{u}) = \lambda(\nabla\cdot\boldsymbol{u})I + \mu(\nabla\boldsymbol{u} + \nabla\boldsymbol{u}^T), \tag{2.1}$$

where $\lambda,\mu>0$ are the Lamé constants of the elastic solid and I is the 3×3 identity matrix. We assume the downward gravitational force to be the only body force acting on the solid medium. The elastic equilibrium of $\mathbb{R}^3_-$ is thus governed by Navier's equation:

$$\nabla\cdot\boldsymbol{\sigma}(\boldsymbol{u}) = -\rho g\hat{\boldsymbol{k}}, \tag{2.2}$$

where g denotes the acceleration of gravity and $\hat{\boldsymbol{k}}$ stands for the unit vector in the direction of positive z-axis. The right-hand side of (2.2) takes into account the effect of the gravity force per unit volume of solid. It has constant magnitude ρg and acts in the direction of $-\hat{\boldsymbol{k}}$ everywhere in $\mathbb{R}^3_-$. As the half-space is unbounded in both horizontal directions x and y, the displacement field due to the gravity force, which we shall call $\boldsymbol{u}_g$, must be in the direction of $-\hat{\boldsymbol{k}}$. On the other hand, it is assumed that the infinite plane surface of the half-space, defined by $z=0$, is traction-free, which is mathematically expressed by homogeneous Neumann boundary conditions:

$$\boldsymbol{\sigma}(\boldsymbol{u})\hat{\boldsymbol{k}} = \boldsymbol{0}. \tag{2.3}$$

It is well-known that under the above hypotheses, the normal stress on horizontal planes due to the weight of the overlying rock increases linearly with depth (cf. [17]). In geosciences, this normal stress is usually called lithostatic (or geostatic) stress. The associated displacement field $\boldsymbol{u}_g$ thus depends quadratically on depth. Furthermore, $\boldsymbol{u}_g$ must satisfy (2.2) and (2.3). The above assumptions lead us to establish that $\boldsymbol{u}_g$ is given by

$$\boldsymbol{u}_g(x,y,z) = -\frac{\rho g z^2}{2(\lambda+2\mu)}\hat{\boldsymbol{k}}. \tag{2.4}$$

Let us suppose next that a hemispherical pit of radius h is dug on the surface of the half-space. We desire to determine to which extent this local perturbation in the geometry affects the elastic equilibrium of the half-space. The geometry of the perturbed semi-infinite domain is described with the aid of a spherical coordinate system (r,ϕ,θ), where r denotes the radial distance, ϕ the polar angle and θ the azimuthal angle. If we place the origin at the centre of the hemispherical pit, the perturbed half-space is described by

$$h<r<\infty, \quad \frac{\pi}{2}<\phi<\pi, \quad 0<\theta<2\pi.$$

This open domain possesses geometric axisymmetry about the vertical axis. Moreover, as the gravity force acts downward, the solid medium can only undergo axisymmetric deformations. The deformed geometry is then independent of θ and we can deal with

https://doi.org/10.4208/aamm.2014.m544 Published online by Cambridge University Press

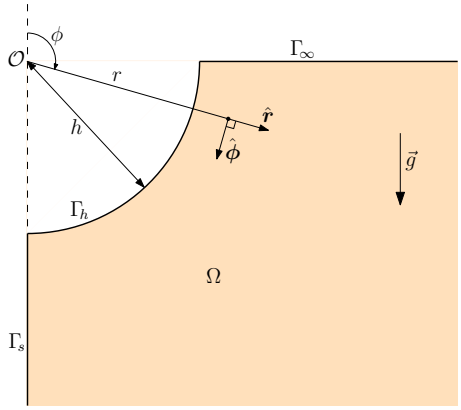


Figure 1: Schematic representation of the axisymmetric semi-infinite domain Ω.

an equivalent domain defined in the (r,ϕ)-plane. We shall denote by Ω the open domain, by Γ_h its hemispherical boundary, by Γ_∞ its infinite horizontal boundary, and by Γ_s its vertical boundary, as indicated in Fig. 1. These sets are defined in terms of (r,ϕ) as follows:

$$\Omega=\{(r,\phi):\, h<r<\infty,\ \pi/2<\phi<\pi\}, \tag{2.5a}$$
$$\Gamma_h=\{(r,\phi):\, r=h,\ \pi/2<\phi<\pi\}, \tag{2.5b}$$
$$\Gamma_\infty=\{(r,\phi):\, r\geq h,\ \phi=\pi/2\}, \tag{2.5c}$$
$$\Gamma_s=\{(r,\phi):\, r\geq h,\ \phi=\pi\}. \tag{2.5d}$$

The displacement field defined in Ω is a vector function $\boldsymbol{u}:\Omega\to\mathbb{R}^2$, which is expressed in terms of its components in r and ϕ as

$$\boldsymbol{u}(r,\phi)=u_r(r,\phi)\hat{\boldsymbol{r}}+u_\phi(r,\phi)\hat{\boldsymbol{\phi}}, \tag{2.6}$$

where $\hat{\boldsymbol{r}}$ and $\hat{\boldsymbol{\phi}}$ stand for the unit vectors in the directions of increasing r and ϕ, respectively (see Fig. 1). In axisymmetric spherical coordinates, the stress tensor $\boldsymbol{\sigma}$ has three non-null normal components σ_r, σ_ϕ, σ_θ, and one non-null shear component $\sigma_{r\phi}$. The remaining two shear components $\sigma_{r\theta}$ and $\sigma_{\phi\theta}$ vanish owing to the axisymmetry. Expressing Hooke's law (2.1) for the non-null components of $\boldsymbol{\sigma}$ yields (cf. [15])

$$\sigma_r(\boldsymbol{u})=(\lambda+2\mu)\frac{\partial u_r}{\partial r}+\frac{\lambda}{r}\left[2u_r+\frac{\partial u_\phi}{\partial\phi}+\cot\phi u_\phi\right], \tag{2.7a}$$
$$\sigma_\phi(\boldsymbol{u})=\lambda\frac{\partial u_r}{\partial r}+\frac{1}{r}\left[2(\lambda+\mu)u_r+(\lambda+2\mu)\frac{\partial u_\phi}{\partial\phi}+\lambda\cot\phi u_\phi\right], \tag{2.7b}$$
$$\sigma_\theta(\boldsymbol{u})=\lambda\frac{\partial u_r}{\partial r}+\frac{1}{r}\left[2(\lambda+\mu)u_r+\lambda\frac{\partial u_\phi}{\partial\phi}+(\lambda+2\mu)\cot\phi u_\phi\right], \tag{2.7c}$$
$$\sigma_{r\phi}(\boldsymbol{u})=\mu\left[\frac{1}{r}\frac{\partial u_r}{\partial\phi}+\frac{\partial u_\phi}{\partial r}-\frac{u_\phi}{r}\right]. \tag{2.7d}$$

https://doi.org/10.4208/aamm.2014.m544 Published online by Cambridge University Press

The elastic equilibrium of the perturbed domain Ω subject to gravity is governed by Navier's equation, given in (2.2). On the other hand, Γ_∞ and Γ_h are both assumed to be traction-free, which means that homogeneous Neumann boundary conditions as those given in (2.3) hold on both boundaries, with $\hat{\boldsymbol{k}}$ substituted by $-\hat{\boldsymbol{r}}$ in the latter case. In addition, the vertical boundary Γ_s is assumed to be free of shear traction and constrained against normal displacement (otherwise the axisymmetry would be destroyed). Furthermore, from physical intuition it is reasonable to assume that the effect of the hemispherical pit on the displacement field in Ω is essentially local, that is, at large distances from the origin the elastic half-space deforms as if there is no geometrical perturbation. We thus assume that, as the distance from the pit tends to infinity, the displacement field $\boldsymbol{u}$ approaches asymptotically $\boldsymbol{u}_g$, i.e., the displacement field in absence of perturbation. An important related issue is the rate at which this asymptotic approach at infinity takes place, which is not a simple matter. It rather concerns questions of existence and uniqueness, which are beyond the scope of this work. We simply assume that when r tends to infinity, the difference in norm between $\boldsymbol{u}$ and $\boldsymbol{u}_g$ decays to zero as $\mathcal{O}(1/r)$, which is sufficient for our purposes. Taking into account all these assumptions, $\boldsymbol{u}$ is obtained as a solution of the boundary-value problem: Find $\boldsymbol{u}:\Omega\to\mathbb{R}^2$ such that

$$\nabla\cdot\boldsymbol{\sigma}(\boldsymbol{u})=-\rho g\hat{\boldsymbol{k}} \qquad \text{in } \Omega, \tag{2.8a}$$
$$\boldsymbol{\sigma}(\boldsymbol{u})\hat{\boldsymbol{k}}=\boldsymbol{0} \qquad \text{on } \Gamma_\infty, \tag{2.8b}$$
$$\boldsymbol{\sigma}(\boldsymbol{u})\hat{\boldsymbol{r}}=\boldsymbol{0} \qquad \text{on } \Gamma_h, \tag{2.8c}$$
$$\boldsymbol{\sigma}(\boldsymbol{u})\hat{\boldsymbol{\phi}}\cdot\hat{\boldsymbol{r}}=\boldsymbol{u}\cdot\hat{\boldsymbol{\phi}}=0 \qquad \text{on } \Gamma_s, \tag{2.8d}$$
$$|\boldsymbol{u}-\boldsymbol{u}_g|=\mathcal{O}\left(\frac{1}{r}\right) \qquad \text{as } r\to\infty, \tag{2.8e}$$

where $|\cdot|$ stands for the Euclidean norm. To solve (2.8), we separate the effect due to the local geometrical perturbation from the effect due to the gravity force in absence of perturbation. This is done by decomposing the displacement field $\boldsymbol{u}$ as

$$\boldsymbol{u}=\boldsymbol{u}_g+\boldsymbol{v}, \tag{2.9}$$

where $\boldsymbol{v}$ is a displacement field to be determined, related to the geometrical perturbation. Replacing (2.9) in (2.8) and combining with (2.4), we obtain that $\boldsymbol{v}$ is a solution of the boundary-value problem: Find $\boldsymbol{v}:\Omega\to\mathbb{R}^2$ such that

$$\nabla\cdot\boldsymbol{\sigma}(\boldsymbol{v})=\boldsymbol{0} \qquad \text{in } \Omega, \tag{2.10a}$$
$$\boldsymbol{\sigma}(\boldsymbol{v})\hat{\boldsymbol{k}}=\boldsymbol{0} \qquad \text{on } \Gamma_\infty, \tag{2.10b}$$
$$\boldsymbol{\sigma}(\boldsymbol{v})\hat{\boldsymbol{r}}=\boldsymbol{f} \qquad \text{on } \Gamma_h, \tag{2.10c}$$
$$\boldsymbol{\sigma}(\boldsymbol{v})\hat{\boldsymbol{\phi}}\cdot\hat{\boldsymbol{r}}=\boldsymbol{v}\cdot\hat{\boldsymbol{\phi}}=0 \qquad \text{on } \Gamma_s, \tag{2.10d}$$
$$|\boldsymbol{v}|=\mathcal{O}\left(\frac{1}{r}\right) \qquad \text{as } r\to\infty, \tag{2.10e}$$

https://doi.org/10.4208/aamm.2014.m544 Published online by Cambridge University Press

where $\boldsymbol{f}:\Gamma_h\to\mathbb{R}^2$ is a vector function defined by its components in r and ϕ as

$$\boldsymbol{f}(\phi)=f_r(\phi)\hat{\boldsymbol{r}}+f_\phi(\phi)\hat{\boldsymbol{\phi}},\quad \frac{\pi}{2}\leq\phi\leq\pi, \tag{2.11}$$

with

$$f_r(\phi)=\rho gh\frac{\left(\nu+(1-2\nu)\cos^2\phi\right)\cos\phi}{1-\nu}, \tag{2.12a}$$

$$f_\phi(\phi)=-\rho gh\frac{(1-2\nu)\cos^2\phi\sin\phi}{1-\nu}, \tag{2.12b}$$

and where $\nu=\lambda/2/(\lambda+\mu)$ denotes the Poisson ratio of the elastic solid. The boundary-value problem (2.10) has certain advantages over (2.8), such as a homogeneous Navier's equation (2.10a) and a solution decaying to zero at infinity (2.10e), which make (2.10) more suitable than (2.8) to be dealt with by analytical techniques. Hence, in order to determine the displacement field $\boldsymbol{u}$, we first solve (2.10) to obtain the displacement field $\boldsymbol{v}$ and then we calculate $\boldsymbol{u}$ from (2.9), given that $\boldsymbol{u}_g$ is given explicitly in (2.4). The procedure to solve (2.10) is thoroughly described in Sections 3 and 4.

3 Analytical solution in series form

In this section, we obtain an analytical solution $\boldsymbol{v}$ in the form of an infinite series, satisfying (2.10a), (2.10b), (2.10d) and (2.10e). The boundary condition on Γ_h, given in (2.10c), is enforced numerically in Section 4. The method employed to obtain this analytical solution is to a certain extent based upon the work by Eubanks [6], but some important modifications and improvements are introduced.

3.1 Boussinesq potentials

First of all, the solution to Navier's equation in Ω is sought with the aid of the so-called Boussinesq potentials, which are a particular case of the more general Papkovich-Neuber (or Boussinesq-Papkovich) representation (cf. [1, 15]). According to [6], $\boldsymbol{v}$ is defined through the following relation

$$2\mu\boldsymbol{v}=\nabla(\Phi+z\Psi)-4(1-\nu)\Psi\hat{\boldsymbol{k}}, \tag{3.1}$$

where Φ and Ψ are the Boussinesq potentials, which are harmonic functions thanks to the fact that Navier's equation (2.10a) is homogeneous. Otherwise, Φ and Ψ would satisfy the Poisson equation, with nonzero right-hand sides. Expressing (3.1) by its components in r and ϕ yields

$$2\mu v_r(r,\phi)=\frac{\partial\Phi}{\partial r}(r,\phi)+r\cos\phi\frac{\partial\Psi}{\partial r}(r,\phi)-(3-4\nu)\cos\phi\Psi(r,\phi), \tag{3.2a}$$

$$2\mu v_\phi(r,\phi)=\frac{1}{r}\frac{\partial\Phi}{\partial\phi}(r,\phi)+\cos\phi\frac{\partial\Psi}{\partial\phi}(r,\phi)+(3-4\nu)\sin\phi\Psi(r,\phi). \tag{3.2b}$$

https://doi.org/10.4208/aamm.2014.m544 Published online by Cambridge University Press

In order to calculate a solution of (2.10a), it becomes necessary to solve the Laplace equation in Ω for Φ and Ψ. Prior to this, we analyse in more detail the decaying condition at infinity for v. By replacing (3.1) in (2.10e), we infer that Φ and Ψ have to satisfy certain asymptotic behaviours when r tends to infinity. Specifically, Ψ has to decay to zero as $\mathcal{O}(1/r)$. It is also required that the term $\nabla(z\Psi)$ appearing in (3.1) decreases to zero at the same rate. We also need that $\nabla\Phi$ decays to zero as $\mathcal{O}(1/r)$, which is a weaker condition than the one required for Ψ. Therefore, Ψ is sought as a solution of

$$\Delta\Psi = 0 \qquad \text{in } \Omega, \tag{3.3a}$$

$$\Psi = \mathcal{O}\left(\frac{1}{r}\right) \qquad \text{as } r\to\infty, \tag{3.3b}$$

and Φ is sought as a solution of

$$\Delta\Phi = 0 \qquad \text{in } \Omega, \tag{3.4a}$$

$$|\nabla\Phi| = \mathcal{O}\left(\frac{1}{r}\right) \qquad \text{as } r\to\infty, \tag{3.4b}$$

where Δ stands for the Laplacian. Let us first determine Ψ. Expressing $\Psi = \Psi(r,\phi)$, the Laplace equation in axisymmetric spherical coordinates is given by

$$\Delta\Psi(r,\phi) = \frac{1}{r^2}\frac{\partial}{\partial r}\left(r^2\frac{\partial\Psi(r,\phi)}{\partial r}\right) + \frac{1}{r^2\sin\phi}\frac{\partial}{\partial\phi}\left(\sin\phi\frac{\partial\Psi(r,\phi)}{\partial\phi}\right) = 0. \tag{3.5}$$

If we apply standard separation of variables in r and ϕ to (3.5) (cf. [3]), and we discard those solutions that are unbounded in Ω, we obtain that for each integer $n\geq 0$, the function Ψ_n defined as

$$\Psi_n(r,\phi) = \frac{P_n(\cos\phi)}{r^{n+1}} \tag{3.6}$$

is a solution of (3.3a), where $P_n(\cdot)$ denotes the Legendre polynomial of order n (see Appendix). The general solution of (3.3a) is then expressed as an infinite linear combination of functions Ψ_n. By virtue of (3.6) it is immediate that

$$\Psi_n(r,\phi) = \mathcal{O}\left(\frac{1}{r^{n+1}}\right) \quad \text{as } r\to\infty,$$

which means that when r increases, the first term of the infinite linear combination (the one for $n=0$) dominates over the rest of the terms, and as this term behaves asymptotically as $\mathcal{O}(1/r)$, the linear combination of all terms behaves asymptotically the same way. Therefore, the obtained general solution of (3.3a) also fulfils the decaying condition (3.3b). In addition, if we compute the terms $\nabla(z\Psi_n)$ for each $n\geq 0$, we verify that

$$|\nabla(z\Psi_n(r,\phi))| = \mathcal{O}\left(\frac{1}{r^{n+1}}\right) \quad \text{as } r\to\infty,$$

https://doi.org/10.4208/aamm.2014.m544 Published online by Cambridge University Press

and an analogous reasoning allows us to state that when r tends to infinity, the term $\nabla(z\Psi)$ decreases asymptotically in norm as $\mathcal{O}(1/r)$. Hence, this term does not affect the fulfilment of (2.10e). Let us now determine Φ. Proceeding analogously as for Ψ, we obtain that the functions Φ_n defined by

$$\Phi_n(r,\phi)=\frac{P_n(\cos\phi)}{r^{n+1}} \tag{3.7}$$

satisfy (3.4a) for each integer $n\geq 0$. As done in [6], it seems reasonable to propose an infinite linear combination of functions Φ_n as the general solution of (3.4a), in analogy to the solution established for (3.3a). Nevertheless, according to the authors' opinion such a solution is not general enough, owing to the decaying condition at infinity (3.4b) imposed on Φ, which differs from that imposed on Ψ. If we calculate the gradients of functions Φ_n defined in (3.7) and we take their norms, it is easy to see that

$$|\nabla\Phi_n(r,\phi)|=\mathcal{O}\left(\frac{1}{r^{n+2}}\right) \quad \text{as} \quad r\to\infty.$$

Consequently, if we express Φ as a linear combination of functions Φ_n defined in (3.7), and if we study the asymptotic behaviour of $|\nabla\Phi|$ as r increases, we obtain that the first term, which is again the dominating one, behaves asymptotically as $\mathcal{O}(1/r^2)$. Thus, when r tends to infinity $|\nabla\Phi|$ decreases to zero as $\mathcal{O}(1/r^2)$. This means that the solution Φ, just expressed as a linear combination of functions Φ_n, satisfies a more restrictive condition than (3.4b), so it is not general enough to be the sought solution of (3.4). In order to achieve the required generality in Φ, we add a new component to the set of functions Φ_n, which gives rise to an asymptotic behaviour of order $\mathcal{O}(1/r)$ in $|\nabla\Phi|$ as r tends to infinity. This component, associated for convenience with the index $n=-1$, corresponds to the following logarithmic potential

$$\Phi_{-1}(r,\phi)=\ln(r-r\cos\phi). \tag{3.8}$$

This potential arises when solving the Boussinesq's problem, i.e., the one of a concentrated force acting normal to the free surface of an elastic half-space (cf. [15]). It is also known as the Boussinesq's elementary solution of the second kind (cf. [1]). It is straightforward to verify that Φ_{-1} is a solution of (3.5). In addition, the singularity of the logarithm at zero in (3.8) does not cause problems of unboundedness, since all those points such that $\cos\phi=1$ (i.e., $\phi=0$) are not contained in the domain Ω. Moreover, if we compute the gradient of Φ_{-1} and we take its norm, we arrive at

$$|\nabla\Phi_{-1}(r,\phi)|=\mathcal{O}\left(\frac{1}{r}\right) \quad \text{as} \quad r\to\infty.$$

Hence, the sought solution to (3.4) corresponds to an infinite linear combination of functions Φ_n including the case $n=-1$, since such a solution satisfies the right decaying condition at infinity (3.4b).

https://doi.org/10.4208/aamm.2014.m544 Published online by Cambridge University Press

3.2 Obtention of the series

Having already solved (3.3) and (3.4), we now resume the obtention of a solution to (2.10) in series form. We have obtained potentials Φ_n, given in (3.7) for $n\geq 0$ and in (3.8) for $n=-1$, and potentials Ψ_n, given in (3.6) for $n\geq 0$. Both kinds of potentials may be combined in different ways in (3.1) or (3.2), giving rise to displacement fields v satisfying (2.10a) and (2.10e). We shall consider two sets of such displacement fields. The first set will consist of displacement fields $v_n^{(1)}$, obtained by setting $\Phi=\Phi_n$ and $\Psi=0$ in (3.1) for $n\geq -1$, that is,

$$2\mu v_n^{(1)}=\nabla\Phi_n, \tag{3.9}$$

whereas the second set will consist of displacement fields $v_n^{(2)}$, obtained by setting $\Psi=(2n+1)\Psi_n$ and $\Phi=-(n-4+4\nu)\Phi_{n-1}$ in (3.1) for $n\geq 0$, that is,

$$2\mu v_n^{(2)}=-(n-4+4\nu)\nabla\Phi_{n-1}+(2n+1)\left[\nabla(z\Psi_n)-4(1-\nu)\Psi_n\hat{\boldsymbol{k}}\right]. \tag{3.10}$$

The reason for considering this particular combination of potentials Φ_n and Ψ_n is that, as stated in [6], the forthcoming calculations are considerably simplified. The general solution to Navier's equation (2.10a) then corresponds to a infinite linear combination of displacement fields $v_n^{(1)}$ and $v_n^{(2)}$, that is,

$$v(r,\phi)=\sum_{n=-1}^{\infty}a_n^{(1)}v_n^{(1)}(r,\phi)+\sum_{n=0}^{\infty}a_n^{(2)}v_n^{(2)}(r,\phi), \tag{3.11}$$

where $a_{-1}^{(1)},a_0^{(1)},a_1^{(1)},\cdots$, and $a_0^{(2)},a_1^{(2)},a_2^{(2)},\cdots$, are unknown real coefficients. Displacement fields $v_n^{(1)}$ and $v_n^{(2)}$ are also expressed in terms of their components in r and ϕ by employing (3.2). Substituting these components in (2.7) yields the components of the stress fields associated with $v_n^{(1)}$ and $v_n^{(2)}$, which we denote respectively by $\sigma_n^{(1)}$ and $\sigma_n^{(2)}$. The stress tensor σ associated with v in (3.11) is thus expressed as

$$\sigma(r,\phi)=\sum_{n=-1}^{\infty}a_n^{(1)}\sigma_n^{(1)}(r,\phi)+\sum_{n=0}^{\infty}a_n^{(2)}\sigma_n^{(2)}(r,\phi). \tag{3.12}$$

Making all the necessary substitutions and rearranging the resulting expressions in each case, we obtain that the displacement fields $v_n^{(1)}$ and $v_n^{(2)}$, together with their associated respective stress fields $\sigma_n^{(1)}$ and $\sigma_n^{(2)}$, can be expressed as

$$v_n^{(1)}(r,\phi)=\frac{1}{r^{n+2}}w_n^{(1)}(\phi),\qquad \sigma_n^{(1)}(r,\phi)=\frac{1}{r^{n+3}}\tau_n^{(1)}(\phi),\qquad n=-1,0,1,\cdots, \tag{3.13a}$$

$$v_n^{(2)}(r,\phi)=\frac{1}{r^{n+1}}w_n^{(2)}(\phi),\qquad \sigma_n^{(2)}(r,\phi)=\frac{1}{r^{n+2}}\tau_n^{(2)}(\phi),\qquad n=0,1,2,\cdots, \tag{3.13b}$$

where $w_n^{(1)}$, $w_n^{(2)}$ are vector functions, and $\tau_n^{(1)}$, $\tau_n^{(2)}$ are tensor functions, all of them depending only on the angle ϕ. This is a convenient form of expressing the displacement

https://doi.org/10.4208/aamm.2014.m544 Published online by Cambridge University Press

and stress fields, since it allows us to make explicit the dependence on r, separating it from the dependence on ϕ. The components of functions $\boldsymbol{w}_n^{(1)}$ and $\boldsymbol{\tau}_n^{(1)}$ for $n=-1$ are

$$2\mu[w_{-1}^{(1)}]_r(\phi)=1, \tag{3.14a}$$
$$2\mu[w_{-1}^{(1)}]_\phi(\phi)=q(\phi)\sin\phi, \tag{3.14b}$$
$$[\tau_{-1}^{(1)}]_r(\phi)=-1, \tag{3.14c}$$
$$[\tau_{-1}^{(1)}]_\phi(\phi)=-q(\phi)\cos\phi, \tag{3.14d}$$
$$[\tau_{-1}^{(1)}]_\theta(\phi)=q(\phi), \tag{3.14e}$$
$$[\tau_{-1}^{(1)}]_{r\phi}(\phi)=-q(\phi)\sin\phi, \tag{3.14f}$$

where the function $q(\cdot)$ is defined as

$$q(\phi)=\frac{1}{1-\cos\phi}, \quad \frac{\pi}{2}\leq\phi\leq\pi. \tag{3.15}$$

The components of functions $\boldsymbol{w}_n^{(1)}$ and $\boldsymbol{\tau}_n^{(1)}$ for $n\geq 0$ are

$$2\mu[w_n^{(1)}]_r(\phi)=-(n+1)P_n(\cos\phi), \tag{3.16a}$$
$$2\mu[w_n^{(1)}]_\phi(\phi)=-\sin\phi P_n'(\cos\phi), \tag{3.16b}$$
$$[\tau_n^{(1)}]_r(\phi)=(n+1)(n+2)P_n(\cos\phi), \tag{3.16c}$$
$$[\tau_n^{(1)}]_\phi(\phi)=P_{n+1}'(\cos\phi)-(n+1)(n+2)P_n(\cos\phi), \tag{3.16d}$$
$$[\tau_n^{(1)}]_\theta(\phi)=-P_{n+1}'(\cos\phi), \tag{3.16e}$$
$$[\tau_n^{(1)}]_{r\phi}(\phi)=(n+2)\sin\phi P_n'(\cos\phi). \tag{3.16f}$$

The components of functions $\boldsymbol{w}_n^{(2)}$ and $\boldsymbol{\tau}_n^{(2)}$ for $n=0$ are

$$2\mu[w_0^{(2)}]_r(\phi)=-4(1-\nu)(1+\cos\phi), \tag{3.17a}$$
$$2\mu[w_0^{(2)}]_\phi(\phi)=-\big(4(1-\nu)q(\phi)-3+4\nu\big)\sin\phi, \tag{3.17b}$$
$$[\tau_0^{(2)}]_r(\phi)=2\big(2-2\nu+(2-\nu)\cos\phi\big), \tag{3.17c}$$
$$[\tau_0^{(2)}]_\phi(\phi)=(4(1-\nu)q(\phi)-1+2\nu)\cos\phi, \tag{3.17d}$$
$$[\tau_0^{(2)}]_\theta(\phi)=-4(1-\nu)q(\phi)-(1-2\nu)\cos\phi, \tag{3.17e}$$
$$[\tau_0^{(2)}]_{r\phi}(\phi)=\big(4(1-\nu)q(\phi)-1+2\nu\big)\sin\phi, \tag{3.17f}$$

and for $n\geq 1$ are

$$2\mu[w_n^{(2)}]_r(\phi)=-(n+1)(n+4-4\nu)P_{n+1}(\cos\phi), \tag{3.18a}$$

https://doi.org/10.4208/aamm.2014.m544 Published online by Cambridge University Press

$$2\mu[w_n^{(2)}]_\phi(\phi) = -(n-3+4\nu)\sin\phi P'_{n+1}(\cos\phi), \tag{3.18b}$$

$$[\tau_n^{(2)}]_r(\phi) = (n+1)\big((n+1)(n+4)-2\nu\big)P_{n+1}(\cos\phi), \tag{3.18c}$$

$$[\tau_n^{(2)}]_\phi(\phi) = -(n+1)(n^2-n+1-2\nu)P_{n+1}(\cos\phi)+(n-3+4\nu)P'_n(\cos\phi), \tag{3.18d}$$

$$[\tau_n^{(2)}]_\theta(\phi) = -(1-2\nu)(n+1)(2n+1)P_{n+1}(\cos\phi)-(n-3+4\nu)P'_n(\cos\phi), \tag{3.18e}$$

$$[\tau_n^{(2)}]_{r\phi}(\phi) = (n^2+2n-1+2\nu)\sin\phi P'_{n+1}(\cos\phi). \tag{3.18f}$$

Substituting (3.13) in (3.11) and (3.12), and grouping terms with the same power of r, we obtain that $\boldsymbol{v}$ and $\boldsymbol{\sigma}$ are also expressed as

$$\boldsymbol{v}(r,\phi) = \sum_{n=-1}^{\infty}\frac{1}{r^{n+2}}\Big(a_n^{(1)}\boldsymbol{w}_n^{(1)}(\phi)+a_{n+1}^{(2)}\boldsymbol{w}_{n+1}^{(2)}(\phi)\Big), \tag{3.19a}$$

$$\boldsymbol{\sigma}(r,\phi) = \sum_{n=-1}^{\infty}\frac{1}{r^{n+3}}\Big(a_n^{(1)}\boldsymbol{\tau}_n^{(1)}(\phi)+a_{n+1}^{(2)}\boldsymbol{\tau}_{n+1}^{(2)}(\phi)\Big). \tag{3.19b}$$

3.3 Traction-free boundary conditions on the plane surface

Next, we impose the traction-free boundary conditions on Γ_∞, given in (2.10b). By virtue of (2.5c), the unit vector $\hat{\boldsymbol{k}}$ coincides with $-\hat{\boldsymbol{\phi}}$ on Γ_∞. Then, it holds that

$$\boldsymbol{\sigma}(\boldsymbol{v})\hat{\boldsymbol{k}} = -\sigma_{r\phi}(\boldsymbol{v})\hat{\boldsymbol{r}}-\sigma_\phi(\boldsymbol{v})\hat{\boldsymbol{\phi}} = \boldsymbol{0} \quad \text{on } \Gamma_\infty.$$

Therefore, components σ_ϕ and $\sigma_{r\phi}$ of (3.19b) must vanish for $\phi=\pi/2$, that is,

$$\sigma_\phi(\boldsymbol{v}) = \sum_{n=-1}^{\infty}\frac{1}{r^{n+3}}\Big(a_n^{(1)}[\tau_n^{(1)}]_\phi\Big(\frac{\pi}{2}\Big)+a_{n+1}^{(2)}[\tau_{n+1}^{(2)}]_\phi\Big(\frac{\pi}{2}\Big)\Big)=0, \tag{3.20a}$$

$$\sigma_{r\phi}(\boldsymbol{v}) = \sum_{n=-1}^{\infty}\frac{1}{r^{n+3}}\Big(a_n^{(1)}[\tau_n^{(1)}]_{r\phi}\Big(\frac{\pi}{2}\Big)+a_{n+1}^{(2)}[\tau_{n+1}^{(2)}]_{r\phi}\Big(\frac{\pi}{2}\Big)\Big)=0. \tag{3.20b}$$

In order to find out under which conditions (3.20a) and (3.20b) hold, we evaluate (3.14d), (3.14f), (3.16d), (3.16f), (3.17d), (3.17f), (3.18d) and (3.18f) at $\phi=\pi/2$. The result varies depending on whether n is even or odd, so we discriminate between these two cases before evaluating the expressions. In the even case, we arrive at

$$[\tau_{2n}^{(1)}]_\phi\Big(\frac{\pi}{2}\Big) = -(2n+1)^2P_{2n}(0), \qquad n\geq 0, \tag{3.21a}$$

$$[\tau_{2n}^{(1)}]_{r\phi}\Big(\frac{\pi}{2}\Big) = 0, \qquad n\geq 0, \tag{3.21b}$$

$$[\tau_{2n}^{(2)}]_\phi\Big(\frac{\pi}{2}\Big) = 0, \qquad n\geq 0, \tag{3.21c}$$

$$[\tau_{2n}^{(2)}]_{r\phi}\Big(\frac{\pi}{2}\Big) = \begin{cases} 3-2\nu, & n=0, \\ (2n+1)\alpha_{2n}P_{2n}(0), & n\geq 1, \end{cases} \tag{3.21d}$$

https://doi.org/10.4208/aamm.2014.m544 Published online by Cambridge University Press

and in the odd case, we obtain

$$[\tau^{(1)}_{2n+1}]_{\phi}\left(\frac{\pi}{2}\right)=0, \qquad n\geq -1, \tag{3.22a}$$

$$[\tau^{(1)}_{2n+1}]_{r\phi}\left(\frac{\pi}{2}\right)=\begin{cases} -1, & n=-1,\\ (2n+1)(2n+3)P_{2n}(0), & n\geq 0, \end{cases} \tag{3.22b}$$

$$[\tau^{(2)}_{2n+1}]_{\phi}\left(\frac{\pi}{2}\right)=(2n+1)\alpha_{2n}P_{2n}(0), \qquad n\geq 0, \tag{3.22c}$$

$$[\tau^{(2)}_{2n+1}]_{r\phi}\left(\frac{\pi}{2}\right)=0, \qquad n\geq 0, \tag{3.22d}$$

where

$$\alpha_{2n}=(2n+1)^2-2(1-\nu),$$

and having combined with (A.5b), (A.5c), (A.5d) and (A.5e) as appropriate. It is easy to verify that by virtue of (3.21) and (3.22), identities (3.20a) and (3.20b) hold, provided that the coefficients $a^{(1)}_n$ and $a^{(2)}_n$ satisfy the relations

$$a^{(1)}_{-1}=(3-2\nu)a^{(2)}_0, \tag{3.23a}$$

$$(2n+1)a^{(1)}_{2n}=\alpha_{2n}a^{(2)}_{2n+1}, \qquad n\geq 0, \tag{3.23b}$$

$$(2n+2)a^{(1)}_{2n+1}=\alpha_{2n+2}a^{(2)}_{2n+2}, \qquad n\geq 0. \tag{3.23c}$$

Thus, separating the infinite sums in (3.19a) and (3.19b) into even and odd terms, and combining with (3.23), we arrive at the following expressions for $\boldsymbol{v}$ and $\boldsymbol{\sigma}$:

$$\begin{aligned}\boldsymbol{v}(r,\phi)=&\frac{a^{(2)}_0}{r}\left((3-2\nu)\boldsymbol{w}^{(1)}_{-1}(\phi)+\boldsymbol{w}^{(2)}_0(\phi)\right)\\ &+\sum_{n=0}^{\infty}\frac{a^{(2)}_{2n+2}}{(2n+2)r^{2n+3}}\left(\alpha_{2n+2}\boldsymbol{w}^{(1)}_{2n+1}(\phi)+(2n+2)\boldsymbol{w}^{(2)}_{2n+2}(\phi)\right)\\ &+\sum_{n=0}^{\infty}\frac{a^{(2)}_{2n+1}}{(2n+1)r^{2n+2}}\left(\alpha_{2n}\boldsymbol{w}^{(1)}_{2n}(\phi)+(2n+1)\boldsymbol{w}^{(2)}_{2n+1}(\phi)\right),\end{aligned} \tag{3.24a}$$

$$\begin{aligned}\boldsymbol{\sigma}(r,\phi)=&\frac{a^{(2)}_0}{r^2}\left((3-2\nu)\boldsymbol{\tau}^{(1)}_{-1}(\phi)+\boldsymbol{\tau}^{(2)}_0(\phi)\right)\\ &+\sum_{n=0}^{\infty}\frac{a^{(2)}_{2n+2}}{(2n+2)r^{2n+4}}\left(\alpha_{2n+2}\boldsymbol{\tau}^{(1)}_{2n+1}(\phi)+(2n+2)\boldsymbol{\tau}^{(2)}_{2n+2}(\phi)\right)\\ &+\sum_{n=0}^{\infty}\frac{a^{(2)}_{2n+1}}{(2n+1)r^{2n+3}}\left(\alpha_{2n}\boldsymbol{\tau}^{(1)}_{2n}(\phi)+(2n+1)\boldsymbol{\tau}^{(2)}_{2n+1}(\phi)\right).\end{aligned} \tag{3.24b}$$

https://doi.org/10.4208/aamm.2014.m544 Published online by Cambridge University Press

This solution satisfies (2.10b), as well as (2.10a) and (2.10e). Defining the vector functions

$$\boldsymbol{w}_n^{(A)}(\phi)=\alpha_{2n}\boldsymbol{w}_{2n}^{(1)}(\phi)+(2n+1)\boldsymbol{w}_{2n+1}^{(2)}(\phi),\qquad n\geq 0, \tag{3.25a}$$

$$\boldsymbol{w}_n^{(B)}(\phi)=\begin{cases}(3-2\nu)\boldsymbol{w}_{-1}^{(1)}(\phi)+\boldsymbol{w}_0^{(2)}(\phi), & n=-1,\\ \alpha_{2n+2}\boldsymbol{w}_{2n+1}^{(1)}(\phi)+(2n+2)\boldsymbol{w}_{2n+2}^{(2)}(\phi), & n\geq 0,\end{cases} \tag{3.25b}$$

and the tensor functions

$$\boldsymbol{\tau}_n^{(A)}(\phi)=\alpha_{2n}\boldsymbol{\tau}_{2n}^{(1)}(\phi)+(2n+1)\boldsymbol{\tau}_{2n+1}^{(2)}(\phi),\qquad n\geq 0, \tag{3.26a}$$

$$\boldsymbol{\tau}_n^{(B)}(\phi)=\begin{cases}(3-2\nu)\boldsymbol{\tau}_{-1}^{(1)}(\phi)+\boldsymbol{\tau}_0^{(2)}(\phi), & n=-1,\\ \alpha_{2n+2}\boldsymbol{\tau}_{2n+1}^{(1)}(\phi)+(2n+2)\boldsymbol{\tau}_{2n+2}^{(2)}(\phi), & n\geq 0,\end{cases} \tag{3.26b}$$

and using the fact that the coefficients $a_n^{(2)}$ are arbitrary, it is possible to reexpress (3.24a) and (3.24b) as

$$\boldsymbol{v}(r,\phi)=\sum_{n=0}^{\infty}A_n\Big(\frac{h}{r}\Big)^{2n+2}\boldsymbol{w}_n^{(A)}(\phi)+\sum_{n=-1}^{\infty}B_n\Big(\frac{h}{r}\Big)^{2n+3}\boldsymbol{w}_n^{(B)}(\phi), \tag{3.27a}$$

$$\boldsymbol{\sigma}(r,\phi)=\frac{1}{h}\Big[\sum_{n=0}^{\infty}A_n\Big(\frac{h}{r}\Big)^{2n+3}\boldsymbol{\tau}_n^{(A)}(\phi)+\sum_{n=-1}^{\infty}B_n\Big(\frac{h}{r}\Big)^{2n+4}\boldsymbol{\tau}_n^{(B)}(\phi)\Big], \tag{3.27b}$$

where A_n and B_n are unknown real coefficients. The components of functions $\boldsymbol{w}_n^{(A)}$, $\boldsymbol{\tau}_n^{(A)}$ for $n=0,1,2,\cdots$, are

$$2\mu[w_n^{(A)}]_r(\phi)=-(2n+1)\big(\alpha_{2n}P_{2n}(\cos\phi)+\gamma_{2n}P_{2n+2}(\cos\phi)\big), \tag{3.28a}$$

$$2\mu[w_n^{(A)}]_\phi(\phi)=-\sin\phi\big(\alpha_{2n}P'_{2n}(\cos\phi)+\epsilon_{2n}P'_{2n+2}(\cos\phi)\big), \tag{3.28b}$$

$$[\tau_n^{(A)}]_r(\phi)=(2n+1)(2n+2)\big(\alpha_{2n}P_{2n}(\cos\phi)+\beta_{2n}P_{2n+2}(\cos\phi)\big), \tag{3.28c}$$

$$\begin{aligned}[\tau_n^{(A)}]_\phi(\phi)=&(\alpha_{2n}+\epsilon_{2n})P'_{2n+1}(\cos\phi)-(2n+1)(2n+2)\\ &\times\big(\alpha_{2n}P_{2n}(\cos\phi)+(\alpha_{2n}-2n+2-4\nu)P_{2n+2}(\cos\phi)\big),\end{aligned} \tag{3.28d}$$

$$\begin{aligned}[\tau_n^{(A)}]_\theta(\phi)=&-(4n+3)\big((2n+1)(2n+2)(1-2\nu)P_{2n+2}(\cos\phi)\\ &+(2n-1+2\nu)P'_{2n+1}(\cos\phi)\big),\end{aligned} \tag{3.28e}$$

$$[\tau_n^{(A)}]_{r\phi}(\phi)=\sin\phi\big((2n+2)\alpha_{2n}P'_{2n}(\cos\phi)+(2n+1)\alpha_{2n+1}P'_{2n+2}(\cos\phi)\big). \tag{3.28f}$$

In the case $n=-1$, the components of functions $\boldsymbol{w}_n^{(B)}$, $\boldsymbol{\tau}_n^{(B)}$ are

$$2\mu[w_{-1}^{(B)}]_r(\phi)=-\big(1-2\nu+4(1-\nu)\cos\phi\big), \tag{3.29a}$$

$$2\mu[w_{-1}^{(B)}]_\phi(\phi)=\sin\phi\big(3-4\nu-(1-2\nu)q(\phi)\big), \tag{3.29b}$$

https://doi.org/10.4208/aamm.2014.m544 Published online by Cambridge University Press

$$[\tau_{-1}^{(B)}]_r(\phi) = 1-2\nu+2(2-\nu)\cos\phi, \tag{3.29c}$$

$$[\tau_{-1}^{(B)}]_\phi(\phi) = -(1-2\nu)\big(1+\cos\phi-q(\phi)\big), \tag{3.29d}$$

$$[\tau_{-1}^{(B)}]_\theta(\phi) = -(1-2\nu)\big(\cos\phi+q(\phi)\big), \tag{3.29e}$$

$$[\tau_{-1}^{(B)}]_{r\phi}(\phi) = -(1-2\nu)\sin\phi\big(1-q(\phi)\big), \tag{3.29f}$$

whereas in the case $n=0,1,2,\cdots$, they are

$$2\mu[w_n^{(B)}]_r(\phi) = -(2n+2)\big(\alpha_{2n+2}P_{2n+1}(\cos\phi)+\gamma_{2n+1}P_{2n+3}(\cos\phi)\big), \tag{3.30a}$$

$$2\mu[w_n^{(B)}]_\phi(\phi) = -\sin\phi\big(\alpha_{2n+2}P'_{2n+1}(\cos\phi)+\epsilon_{2n+1}P'_{2n+3}(\cos\phi)\big), \tag{3.30b}$$

$$[\tau_n^{(B)}]_r(\phi) = (2n+2)(2n+3)\big(\alpha_{2n+2}P_{2n+1}(\cos\phi)+\beta_{2n+1}P_{2n+3}(\cos\phi)\big), \tag{3.30c}$$

$$\begin{aligned}[\tau_n^{(B)}]_\phi(\phi) = {}& \big(\alpha_{2n+2}+\epsilon_{2n+1}\big)P'_{2n+2}(\cos\phi)-(2n+2)(2n+3)\\ &\times\big(\alpha_{2n+2}P_{2n+1}(\cos\phi)+(\alpha_{2n+1}-2n+1-4\nu)P_{2n+3}(\cos\phi)\big),\end{aligned} \tag{3.30d}$$

$$\begin{aligned}[\tau_n^{(B)}]_\theta(\phi) = {}& -(4n+5)\big((2n+2)(2n+3)(1-2\nu)P_{2n+3}(\cos\phi)\\ &+(2n+1+2\nu)P'_{2n+2}(\cos\phi)\big),\end{aligned} \tag{3.30e}$$

$$[\tau_n^{(B)}]_{r\phi}(\phi) = \sin\phi\alpha_{2n+2}\big((2n+3)P'_{2n+1}(\cos\phi)+(2n+2)P'_{2n+3}(\cos\phi)\big), \tag{3.30f}$$

where the coefficients β_{2n}, γ_{2n} and ϵ_{2n} are defined as

$$\beta_{2n} = (2n+2)(2n+5)-2\nu, \quad \gamma_{2n} = (2n+2)(2n+5-4\nu), \quad \epsilon_{2n} = (2n+1)(2n-2+4\nu).$$

3.4 Axisymmetric boundary conditions

Let us briefly analyse the fulfilment of the axisymmetric boundary conditions on Γ_s, given in (2.10d). We have that

$$\boldsymbol{\sigma}(\boldsymbol{v})\hat{\boldsymbol{\phi}}\cdot\hat{\boldsymbol{r}} = (\sigma_{r\phi}(\boldsymbol{v})\hat{\boldsymbol{r}}+\sigma_\phi(\boldsymbol{v})\hat{\boldsymbol{\phi}})\cdot\hat{\boldsymbol{r}} = \sigma_{r\phi}(\boldsymbol{v}), \tag{3.31}$$

and

$$\boldsymbol{v}\cdot\hat{\boldsymbol{\phi}} = v_\phi, \tag{3.32}$$

so we need that the component v_ϕ of (3.27a) and the component $\sigma_{r\phi}$ of (3.27b) vanish on Γ_∞, that is, for $\phi=\pi$ (cf. (2.5b)). Actually, these conditions are already fulfilled due to the factor $\sin\phi$ existing in (3.28b), (3.28f), (3.29b), (3.29f), (3.30b) and (3.30f). Consequently, the analytical solution given in (3.27a)-(3.27b) satisfies also (2.10d). In the next section, we impose the boundary conditions on Γ_h, given in (2.10c).

4 Numerical enforcement of boundary conditions on the hemispherical pit

Up to now, we have obtained a solution in series form, given in (3.27a)-(3.27b), which satisfies the elasticity equation (2.10a), the traction-free boundary conditions on the infi-

https://doi.org/10.4208/aamm.2014.m544 Published online by Cambridge University Press

nite plane surface (2.10b), the axisymmetric boundary conditions on the vertical surface (2.10d), and the decaying condition at infinity (2.10e). It is a fully analytical solution, since no numerical approximation has been introduced yet. In the present section, we enforce this solution to satisfy the boundary conditions on the hemispherical surface (2.10c), which is only possible in numerical form, so the sought solution becomes semi-analytical. This numerical enforcement is done by means of minimising a quadratic functional, as described below.

4.1 Truncation of the series

The fulfilment of the boundary conditions on the pit (2.10c) is directly related to the coefficients A_n and B_n in (3.27a)-(3.27b), which have to be chosen in such a way that (2.10c) is satisfied. However, there is an infinite number of coefficients A_n and B_n, which are determined by an infinite set of simultaneous linear equations. Hence, it is not possible to calculate them exactly, keeping the analytical nature of the solution. This drawback is overcome by truncating the infinite series in (3.27a)-(3.27b) at a finite order N, which introduces the first numerical approximation to our procedure and gives rise to a semi-analytical solution of (2.10). The truncated solution is given by

$$\boldsymbol{v}_N(r,\phi)=\sum_{n=0}^{N}A_n\left(\frac{h}{r}\right)^{2n+2}\boldsymbol{w}_n^{(A)}(\phi)+\sum_{n=-1}^{N}B_n\left(\frac{h}{r}\right)^{2n+3}\boldsymbol{w}_n^{(B)}(\phi), \tag{4.1a}$$

$$\boldsymbol{\sigma}_N(r,\phi)=\frac{1}{h}\Big[\sum_{n=0}^{N}A_n\left(\frac{h}{r}\right)^{2n+3}\boldsymbol{\tau}_n^{(A)}(\phi)+\sum_{n=-1}^{N}B_n\left(\frac{h}{r}\right)^{2n+4}\boldsymbol{\tau}_n^{(B)}(\phi)\Big]. \tag{4.1b}$$

This approximation fixes a finite number of coefficients A_n and B_n that are to be calculated. This is done by solving a finite linear system of equations for the coefficients A_n and B_n, which is obtained next.

4.2 Quadratic functional and its matrix form

The method to determine a linear system of equations satisfied by the coefficients A_n and B_n is based upon the minimisation of a quadratic functional, which we define as

$$J(\boldsymbol{v}_N)=-\frac{1}{2h^2}\int_{\Gamma_h}\boldsymbol{\sigma}_N\hat{\boldsymbol{r}}\cdot\boldsymbol{v}_N\mathrm{d}s+\frac{1}{h^2}\int_{\Gamma_h}\boldsymbol{f}\cdot\boldsymbol{v}_N\mathrm{d}s, \tag{4.2}$$

where $\boldsymbol{v}_N$ and $\boldsymbol{\sigma}_N$ are given in (4.1a) and (4.1b), respectively, and $\boldsymbol{f}$ is the vector function that arises at the right-hand side of (2.10c), whose components in r and ϕ were defined in (2.12a) and (2.12b), respectively. The first term in the right-hand side of (4.2) is quadratic in $\boldsymbol{v}_N$ and represents the surface elastic potential energy on Γ_h. The minus sign has been chosen in order to obtain a strictly convex functional. The second term is linear in $\boldsymbol{v}_N$ and is related to the right-hand side vector function $\boldsymbol{f}$. Although we have assumed a particular function $\boldsymbol{f}$, the subsequent analysis is valid for any piecewise continuous function

https://doi.org/10.4208/aamm.2014.m544 Published online by Cambridge University Press

$\boldsymbol{f}:\Gamma_h\to\mathbb{R}^2$ satisfying $f_\phi(\pi)=0$. Moreover, $\boldsymbol{v}_N$ and $\boldsymbol{\sigma}_N$ are regarded in (4.2) as generic functions depending on the arbitrary coefficients $A_0,A_1,A_2,\cdots,A_N$ and $B_{-1},B_0,B_1,\cdots,B_N$, respectively, which are to be determined in order to minimise the functional J. Expressing $\boldsymbol{v}_N$, $\boldsymbol{\sigma}_N$ and $\boldsymbol{f}$ in terms of their respective components in r and ϕ, making explicit the integrals and rearranging terms, (4.2) is rewritten as

$$\begin{aligned}J(\boldsymbol{v}_N)=&-\frac{1}{2}\int_{\pi/2}^{\pi}\left([\sigma_N]_r(h,\phi)[v_N]_r(h,\phi)+[\sigma_N]_{r\phi}(h,\phi)[v_N]_\phi(h,\phi)\right)\sin\phi\mathrm{d}\phi\\&+\int_{\pi/2}^{\pi}\left(f_r(h,\phi)[v_N]_r(h,\phi)+f_\phi(h,\phi)[v_N]_\phi(h,\phi)\right)\sin\phi\mathrm{d}\phi,\end{aligned}\tag{4.3}$$

and next, the components of $\boldsymbol{v}_N$ and $\boldsymbol{\sigma}_N$ in (4.1a) and (4.1b) are evaluated at $r=h$ and substituted in (4.3). Expanding the resulting terms and collecting the products A_nA_k, A_nB_k, B_nA_k and B_nB_k, the functional J is reexpressed as

$$\begin{aligned}J(\boldsymbol{v}_N)=&\frac{1}{2}\sum_{n=0}^{N}\sum_{k=0}^{N}Q_{nk}^{(AA)}A_nA_k+\frac{1}{2}\sum_{n=0}^{N}\sum_{k=-1}^{N}Q_{nk}^{(AB)}A_nB_k+\frac{1}{2}\sum_{n=-1}^{N}\sum_{k=0}^{N}Q_{nk}^{(BA)}B_nA_k\\&+\frac{1}{2}\sum_{n=-1}^{N}\sum_{k=-1}^{N}Q_{nk}^{(BB)}B_nB_k-\sum_{n=0}^{N}c_n^{(A)}A_n-\sum_{n=-1}^{N}c_n^{(B)}B_n,\end{aligned}\tag{4.4}$$

where the terms $Q_{nk}^{(AA)}$, $Q_{nk}^{(AB)}$, $Q_{nk}^{(BA)}$, $Q_{nk}^{(BB)}$, $c_n^{(A)}$ and $c_n^{(B)}$ correspond to the entries of matrices $\boldsymbol{Q}^{(AA)}\in\mathbf{M}_{N+1}(\mathbb{R})$, $\boldsymbol{Q}^{(AB)}\in\mathbf{M}_{(N+1)\times(N+2)}(\mathbb{R})$, $\boldsymbol{Q}^{(BA)}\in\mathbf{M}_{(N+2)\times(N+1)}(\mathbb{R})$, $\boldsymbol{Q}^{(BB)}\in\mathbf{M}_{N+2}(\mathbb{R})$ and vectors $\boldsymbol{c}^{(A)}\in\mathbb{R}^{N+1}$ and $\boldsymbol{c}^{(B)}\in\mathbb{R}^{N+2}$, respectively. These entries are defined as the following integrals:

$$Q_{nk}^{(ij)}=-\int_{\pi/2}^{\pi}\left([w_n^{(i)}]_r(\phi)[\tau_k^{(j)}]_r(\phi)+[w_n^{(i)}]_\phi(\phi)[\tau_k^{(j)}]_{r\phi}(\phi)\right)\sin\phi\mathrm{d}\phi,\tag{4.5a}$$

$$c_n^{(i)}=-h\int_{\pi/2}^{\pi}\left([w_n^{(i)}]_r(\phi)f_r(\phi)+[w_n^{(i)}]_\phi(\phi)f_\phi(\phi)\right)\sin\phi\mathrm{d}\phi,\tag{4.5b}$$

where $i,j=A,B$. Substituting Eqs. (2.12a), (2.12b), (3.28a), (3.28b), (3.28c), (3.28f), (3.29a), (3.29b), (3.29c), (3.29f), (3.30a), (3.30b), (3.30c), (3.30f) in (4.5a) and (4.5b) as appropriate leads us to obtain expressions for the quantities $Q_{nk}^{(ij)}$ and $c_n^{(i)}$ in terms of explicit integrals. These expressions are too cumbersome to be reproduced here. However, with the aid of the integral formulae provided in the Appendix, all the involved integrals are calculated exactly, yielding explicit expressions for the entries of matrices $\boldsymbol{Q}^{(ij)}$ and vectors $\boldsymbol{c}^{(i)}$ which we reproduce next for $i,j=A,B$. The entries of the matrix $\boldsymbol{Q}^{(AA)}$ are computed by using (A.6a) and (A.6d), corresponding to a tridiagonal symmetric matrix with main diagonal entries

$$\begin{aligned}Q_{nn}^{(AA)}=&\frac{(2n+1)(2n+2)(4n+3)}{(4n+5)}\\&\times\left((2n+3)(16n^3+32n^2+22n+8\nu^2-12\nu+9)+4(1-\nu^2)\right),\end{aligned}\tag{4.6}$$

https://doi.org/10.4208/aamm.2014.m544 Published online by Cambridge University Press

where $0\leq n\leq N$, and sub-diagonal and super-diagonal entries

$$Q^{(AA)}_{n,n+1}=Q^{(AA)}_{n+1,n}=\frac{(2n+1)(2n+2)(2n+3)(2n+4)(4n+3)}{(4n+5)}\times\big((2n+2)(2n+4)-1+2\nu\big),\tag{4.7}$$

where $0\leq n\leq N-1$. The entries of matrices $\boldsymbol{Q}^{(AB)}$ and $\boldsymbol{Q}^{(BA)}$ are calculated by using (A.6a), (A.6c), (A.6f) and (A.7a). It is obtained that they correspond to full matrices satisfying $\boldsymbol{Q}^{(BA)}=[\boldsymbol{Q}^{(AB)}]^T$. The entries of $\boldsymbol{Q}^{(AB)}$ in the case $k=-1$ are given by

$$Q^{(AB)}_{n,-1}=-\frac{4(4n+3)(2n(2n+3)\nu(\nu-2)-3+5\nu-4\nu^2)P_{2n}(0)}{(2n-1)(2n+2)(2n+4)},\tag{4.8}$$

and in the case $0\leq k\leq N+1$ are given by

$$Q^{(AB)}_{nk}=\frac{4(2k+1)(2k+3)(4k+5)(2n+1)(4n+3)\eta_{nk}P_{2n}(0)P_{2k}(0)}{(2k+6+2n)(2k+3-2n)(2k+4+2n)(2k-1-2n)(2k+1-2n)},\tag{4.9}$$

where

$$\begin{aligned}\eta_{nk}=&\,51+58k+32k^2n^2+188kn+138n+56k^2n+72n^2+16k^2+104kn^2\\&-\big((2k-1-2n)\big(4n^2(2k+4)-4k((2k+5)n+2k+6)-21\big)-8k(2k+2)\big)\nu\\&-(2k+3-2n)(2k+6+2n)(2k-1-2n)\nu^2,\end{aligned}$$

and $0\leq n\leq N$. The entries of matrix $\boldsymbol{Q}^{(BB)}$ are calculated by using (A.6b), (A.6c), (A.6e), and (A.7b), together with some elementary primitives of trigonometric functions. It is obtained that $\boldsymbol{Q}^{(BB)}$ corresponds to a symmetric matrix that is almost tridiagonal, except for its first row and its first column, which are full. The entries associated with the first row and column of $\boldsymbol{Q}^{(BB)}$ are

$$Q^{(BB)}_{-1,-1}=2(1-2\nu)^2\ln 2+\frac{2}{3}(2+5\nu-6\nu^2),\tag{4.10a}$$

$$Q^{(BB)}_{n,-1}=Q^{(BB)}_{-1,n}=-\frac{2(1-2\nu)(4n+5)(2n+1)\big((2n+4)\nu-1\big)P_{2n}(0)}{(2n+2)(2n+4)}+2(7+2\nu)\delta_{n0},\tag{4.10b}$$

where $0\leq n\leq N$ and δ_{nk} stands for the Kronecker delta. The entries associated with the tridiagonal part of $\boldsymbol{Q}^{(BB)}$ are the main diagonal entries

$$Q^{(BB)}_{nn}=\frac{(4n+5)(2n+2)(2n+3)}{(4n+7)}\times(32n^4+208n^3+492n^2+4(125-2\nu+4\nu^2)n+187-20\nu+28\nu^2),\tag{4.11}$$

https://doi.org/10.4208/aamm.2014.m544 Published online by Cambridge University Press

where $0 \leq n \leq N$, and the and sub-diagonal and super-diagonal entries

$$Q^{(BB)}_{n+1,n} = Q^{(BB)}_{n,n+1} = \frac{(4n+5)(2n+2)(2n+3)(2n+4)(2n+5)}{(4n+7)} \times ((2n+4)(2n+6)-1+2\nu), \tag{4.12}$$

where $0 \leq n \leq N-1$. The entries of vector $\boldsymbol{c}^{(A)}$ are computed by using (A.6c) and (A.6f), yielding

$$c^{(A)}_n = \frac{2\rho g h^2 (4n+3)(2n+1) P_{2n}(0)}{(1-\nu)(2n-1)(2n+2)(2n+4)(2n+6)} \times (4(2n+3) - 6\nu(3n+5) + \nu^2(2n+4)(2n+6)), \tag{4.13}$$

where $0 \leq n \leq N$. The entries of vector $\boldsymbol{c}^{(B)}$ are computed by using Eqs. (A.6b), (A.6c), (A.6e) and (A.7b). It is obtained that only the first two entries of $\boldsymbol{c}^{(B)}$ are different from zero. These entries are given by

$$c^{(B)}_{-1} = \frac{\rho g h^2 (26 - 47\nu + 30\nu^2)}{30(1-\nu)}, \quad c^{(B)}_0 = \frac{2\rho g h^2 (46 - 71\nu + 70\nu^2)}{21(1-\nu)}. \tag{4.14}$$

We define also the vectors $\boldsymbol{x}^{(A)} \in \mathbb{R}^{N+1}$ and $\boldsymbol{x}^{(B)} \in \mathbb{R}^{N+2}$ as those whose entries correspond to the coefficients A_n and B_n to be computed, that is,

$$x^{(A)}_n = A_n, \qquad 0 \leq n \leq N, \tag{4.15a}$$

$$x^{(B)}_n = B_n, \qquad -1 \leq n \leq N. \tag{4.15b}$$

From the above matrices and vectors, we also define the square matrix $\boldsymbol{Q} \in \mathbf{M}_{2N+3}(\mathbb{R})$ and the vectors $\boldsymbol{x}, \boldsymbol{c} \in \mathbb{R}^{2N+3}$ by blocks as

$$\boldsymbol{Q} = \begin{bmatrix} \boldsymbol{Q}^{(AA)} & \boldsymbol{Q}^{(AB)} \\ [\boldsymbol{Q}^{(AB)}]^T & \boldsymbol{Q}^{(BB)} \end{bmatrix}, \quad \boldsymbol{x} = \begin{bmatrix} \boldsymbol{x}^{(A)} \\ \boldsymbol{x}^{(B)} \end{bmatrix}, \quad \boldsymbol{c} = \begin{bmatrix} \boldsymbol{c}^{(A)} \\ \boldsymbol{c}^{(B)} \end{bmatrix}, \tag{4.16}$$

which allow us to reexpress the functional J given in (4.4) as the following quadratic form in $\boldsymbol{x}$:

$$J(\boldsymbol{x}) = \frac{1}{2}\boldsymbol{x}^T \boldsymbol{Q} \boldsymbol{x} - \boldsymbol{x}^T \boldsymbol{c}. \tag{4.17}$$

4.3 Linear system and method of inversion

A linear system for the coefficients A_n and B_n is obtained by minimisation of the functional J. It holds that $\boldsymbol{Q}$ is a symmetric matrix, due to the properties of its blocks $\boldsymbol{Q}^{(ij)}$, and it is also positive definite, thanks to the elliptic nature of the elastostatic boundary-value

https://doi.org/10.4208/aamm.2014.m544 Published online by Cambridge University Press

problem. Therefore, J has a global minimum, which is reached when $\nabla J(\boldsymbol{x}) = \boldsymbol{Q}\boldsymbol{x} - \boldsymbol{c} = \boldsymbol{0}$, or equivalently, when

$$\boldsymbol{Q}\boldsymbol{x} = \boldsymbol{c}. \tag{4.18}$$

Eq. (4.18) corresponds to the sought linear system of equations for the coefficients A_n and B_n. We take advantage of the symmetry and positive definiteness of $\boldsymbol{Q}$ in solving (4.18). Expressing $\boldsymbol{Q}$, $\boldsymbol{x}$ and $\boldsymbol{c}$ by blocks in (4.18) yields

$$\begin{bmatrix} \boldsymbol{Q}^{(AA)} & \boldsymbol{Q}^{(AB)} \\ [\boldsymbol{Q}^{(AB)}]^T & \boldsymbol{Q}^{(BB)} \end{bmatrix} \begin{bmatrix} \boldsymbol{x}^{(A)} \\ \boldsymbol{x}^{(B)} \end{bmatrix} = \begin{bmatrix} \boldsymbol{c}^{(A)} \\ \boldsymbol{c}^{(B)} \end{bmatrix}, \tag{4.19}$$

and this system is inverted with the aid of the so-called Schur-Banachiewicz blockwise inversion formula (cf. [5]), which is given by

$$\begin{aligned} \boldsymbol{x}^{(A)} &= \big([\boldsymbol{Q}^{(AA)}]^{-1} + [\boldsymbol{Q}^{(AA)}]^{-1}\boldsymbol{Q}^{(AB)}[\widetilde{\boldsymbol{Q}}^{(BB)}]^{-1}[\boldsymbol{Q}^{(AB)}]^T[\boldsymbol{Q}^{(AA)}]^{-1}\big)\boldsymbol{c}^{(A)} \\ &\quad - [\boldsymbol{Q}^{(AA)}]^{-1}\boldsymbol{Q}^{(AB)}[\widetilde{\boldsymbol{Q}}^{(BB)}]^{-1}\boldsymbol{c}^{(B)}, \end{aligned} \tag{4.20a}$$

$$\boldsymbol{x}^{(B)} = -[\widetilde{\boldsymbol{Q}}^{(BB)}]^{-1}[\boldsymbol{Q}^{(AB)}]^T[\boldsymbol{Q}^{(AA)}]^{-1}\boldsymbol{c}^{(A)} + [\widetilde{\boldsymbol{Q}}^{(BB)}]^{-1}\boldsymbol{c}^{(B)}, \tag{4.20b}$$

where $\widetilde{\boldsymbol{Q}}^{(BB)}$ denotes the Schur complement of $\boldsymbol{Q}^{(BB)}$ in $\boldsymbol{Q}$, defined as

$$\widetilde{\boldsymbol{Q}}^{(BB)} = \boldsymbol{Q}^{(BB)} - [\boldsymbol{Q}^{(AB)}]^T[\boldsymbol{Q}^{(AA)}]^{-1}\boldsymbol{Q}^{(AB)}. \tag{4.21}$$

To evaluate (4.20a) and (4.20b), it suffices to inverse the symmetric and positive definite matrices $\boldsymbol{Q}^{(AA)}$ and $\widetilde{\boldsymbol{Q}}^{(BB)}$. As $\boldsymbol{Q}^{(AA)}$ is in addition a tridiagonal matrix, it is efficiently inverted by using the Thomas algorithm for tridiagonal systems (cf. [11], Algorithm 4.3.6). To invert $\widetilde{\boldsymbol{Q}}^{(BB)}$, we employ its Cholesky factorisation, which is quickly obtained with the aid of a suitable algorithm (cf. [11], Algorithm 4.2.1). We thus establish the following algorithm to compute the coefficients A_n and B_n:

1. Compute the coefficients for tridiagonal inversion of $\boldsymbol{Q}^{(AA)}$.
2. Use the coefficients to evaluate $[\boldsymbol{Q}^{(AA)}]^{-1}\boldsymbol{c}^{(A)}$ and $[\boldsymbol{Q}^{(AA)}]^{-1}\boldsymbol{Q}^{(AB)}$.
3. Calculate the Schur complement $\widetilde{\boldsymbol{Q}}^{(BB)}$ using (4.21).
4. Obtain the Cholesky factorisation of $\widetilde{\boldsymbol{Q}}^{(BB)}$.
5. Use the Cholesky factorisation to evaluate $[\widetilde{\boldsymbol{Q}}^{(BB)}]^{-1}\boldsymbol{c}^{(B)}$ and $[\widetilde{\boldsymbol{Q}}^{(BB)}]^{-1}[\boldsymbol{Q}^{(AB)}]^T$.
6. Assemble $\boldsymbol{x}^{(A)}$ and $\boldsymbol{x}^{(B)}$ as indicated in (4.20a) and (4.20b).

This algorithm yields approximate values of the coefficients $A_0, A_1, A_2, \cdots, A_N$ and $B_{-1}, B_0, B_1, \cdots, B_N$. By substituting these values in (4.1a) and (4.1b), we obtain the desired semi-analytical solution of the boundary-value problem (2.10) in explicit way.

https://doi.org/10.4208/aamm.2014.m544 Published online by Cambridge University Press

5 Numerical results and validation

In this section, we present numerical results obtained with the semi-analytical method described throughout Sections 3 and 4. Prior to this, the convergence of the series is numerically verified and a convergence criterion is established in order to determine a suitable value for the truncation parameter N. Furthermore, the procedure is validated by comparing our semi-analytical solution with results obtained numerically using the commercial software COMSOL Multiphysics. The unbounded domain Ω is truncated by means of an artificial square box.

5.1 Numerical results

The semi-analytical method described in Sections 3 and 4 was implemented in its entirety, and the obtained solution was numerically evaluated for different values of N. The considered numerical values of the gravity acceleration g, the radius of the pit h, the density ρ, the Young's modulus E and the Poisson's ratio ν are shown in Table 1. The chosen values of ρ, E and ν are in the range of common rock properties (see [16] for details). The Lamé's parameters λ and μ are easily obtained from E and ν through the usual formulae

$$\lambda=\frac{\nu E}{(1+\nu)(1-2\nu)},\quad \mu=\frac{E}{2(1+\nu)}. \tag{5.1}$$

To evaluate numerically the semi-analytical solution of (2.10) and analyse its convergence as the truncation parameter N tends to infinity, we consider a bounded subregion of Ω, defined in axisymmetric spherical coordinates by the points (r,ϕ) satisfying $h\leq r\leq 2000$ m and $\pi/2\leq\phi\leq\pi$. The evaluations are performed at the points (r_i,ϕ_j) of an equispaced rectangular grid in the (r,ϕ)-plane, defined as $r_i=h+i\Delta r$ and $\phi_j=\pi/2+j\Delta\phi$, where $i=0,1,2,\cdots,140$, $\Delta r=10$m, $j=0,1,2,\cdots,500$, and $\Delta\phi=\pi/1000$. In order to test numerically the convergence of the series in terms of N, we compute the relative error between two successive solutions, considering separately the displacement field $\boldsymbol{v}$ and the stress tensor $\boldsymbol{\sigma}(\boldsymbol{v})$. The respective relative errors are defined as

$$e_N(\boldsymbol{v})=\frac{|\boldsymbol{v}_{N+1}-\boldsymbol{v}_N|}{|\boldsymbol{v}_N|},\quad e_N(\boldsymbol{\sigma})=\frac{|\boldsymbol{\sigma}_{N+1}(\boldsymbol{v}_{N+1})-\boldsymbol{\sigma}_N(\boldsymbol{v}_N)|}{|\boldsymbol{\sigma}_N(\boldsymbol{v}_N)|}, \tag{5.2}$$

where in the latter case, $|\cdot|$ corresponds to the matrix Euclidean norm (or Frobenius norm). Successive values of the truncation parameter up to $N=100$ were considered in the analysis. A semi-logarithmic plot with both relative errors in function of N is presented in Fig. 2, where it is observed that both of them decrease as N increases, exhibiting the

Table 1: Numerical values of the physical parameters.

Parameter	h	g	ρ	E	ν
Value	600 m	9.81 m/s^2	2725 Kg/m^3	70.2 GPa	0.3

https://doi.org/10.4208/aamm.2014.m544 Published online by Cambridge University Press

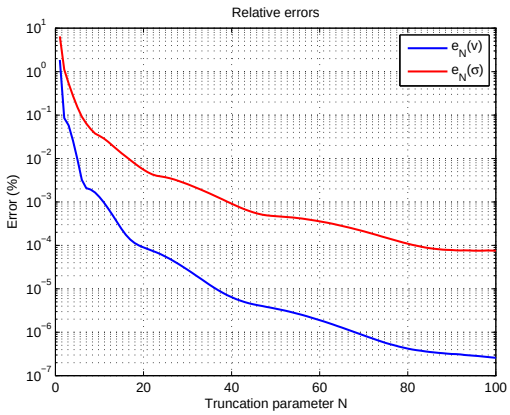


Figure 2: Relative error of the solution between two successive iterations in N.

error associated with the stress tensor a slower decrease. We conclude from this analysis that the semi-analytical method shows an acceptable convergence. In order to set a value of N for evaluation of the semi-analytical solution, we have used as a convergence criterion that both relative errors have to be smaller than a tolerance of 0.001%, yielding the value $N=40$ (see Fig. 2), which we assume from now on. Having already calculated the solution $\boldsymbol{v}$, the physical displacement field $\boldsymbol{u}$ is obtained by adding the lithostatic displacement field $\boldsymbol{u}_g$ (evaluated at the same rectangular grid), as indicated in (2.9). The physical stress tensor $\boldsymbol{\sigma}(\boldsymbol{u})$ is obtained in a similar way, by adding to $\boldsymbol{\sigma}(\boldsymbol{v})$ the lithostatic stress tensor $\boldsymbol{\sigma}(\boldsymbol{u}_g)$, whose components are explicitly obtained by substituting (2.4) in (2.7). The values of the displacement components u_r and u_ϕ, and the stress components $\sigma_r(\boldsymbol{u})$, $\sigma_\phi(\boldsymbol{u})$, $\sigma_\theta(\boldsymbol{u})$ and $\sigma_{r\phi}(\boldsymbol{u})$ are depicted in Fig. 3. It is observed from the plots of stress components that obtained semi-analytical solution fulfils the boundary conditions (2.8b), (2.8c) and (2.8d).

5.2 Validation of the procedure

In order to confirm the correctness of the semi-analytical solution, a validation test was carried out. For this, the axisymmetric boundary-value problem in $\boldsymbol{u}$ (2.8) was numerically solved using the commercial finite element software COMSOL Multiphysics, with the physical parameters of the problem fixed to the same numerical values indicated in Table 1. The purpose of this numerical simulation is to compare the results calculated by such means with those obtained by using the semi-analytical method proposed herein. As this type of software is only able to deal with bounded regions, the unbounded domain Ω was truncated by means of an artificial square box of length L, as indicated schematically in Fig. 4. In order to be able to solve (2.8) in the truncated domain (denoted by Ω_{tr}), the decaying condition at infinity (2.8e) was replaced by artificial Dirichlet boundary conditions on the right and bottom boundaries, with the displacements set to the lithostatic displacement $\boldsymbol{u}_g$ field given in (2.4). Different values of the length L

https://doi.org/10.4208/aamm.2014.m544 Published online by Cambridge University Press

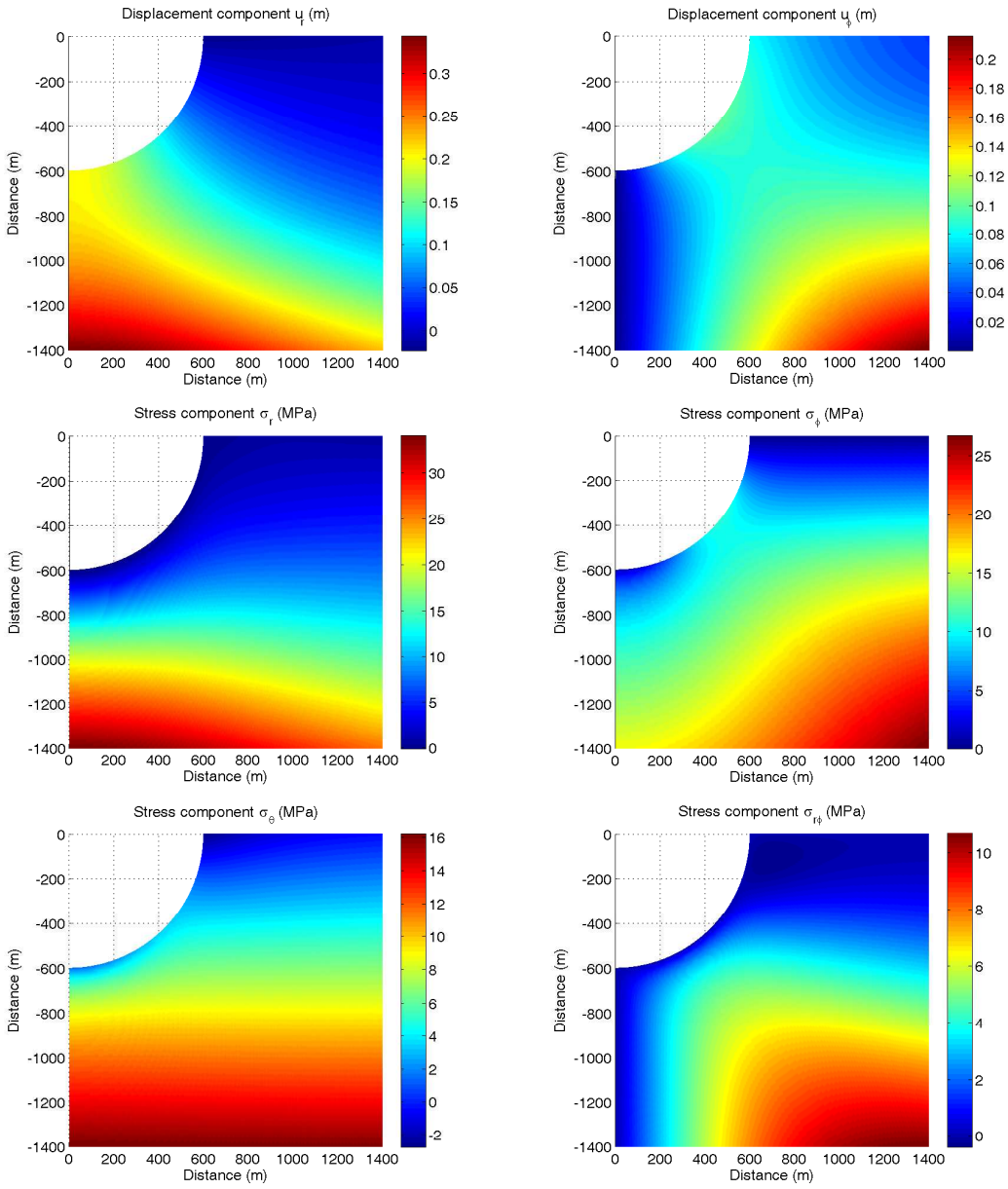


Figure 3: Plots of displacement and stress components obtained in Ω.

were considered, starting from a minimum value of $L=1000$m up to a maximum value of $L=13000$m, with successive increases of $\Delta L=1000$m. For each one of these values, non-uniform triangular meshes of the domain Ω_{tr} were generated, with the element size varying between a minimum value of 2m and a maximum value of 50m, and the maximum element growth rate set to 1.3. To solve numerically the boundary-value problem, standard

https://doi.org/10.4208/aamm.2014.m544 Published online by Cambridge University Press

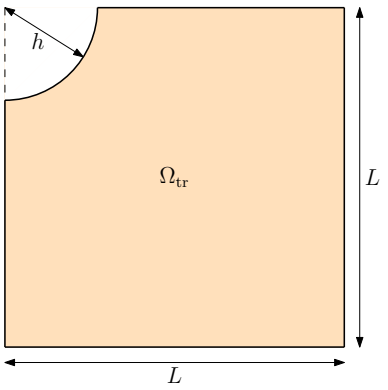


Figure 4: Schematic representation of the domain Ω truncated by a square box of length L.

conforming P1 finite elements in each mesh were used. Common sense indicates that as the domain size grows, the approximation of the unbounded boundary-value problem (2.8) by a bounded one becomes more accurate. Therefore, it is expected that the solution calculated numerically by finite elements approaches the semi-analytical solution as the length L increases. In order to find out whether this occurs, the displacement components u_r and u_ϕ, and the stress components σ_ϕ and σ_θ obtained by both means were compared on the surface of the pit Γ_h. The remaining stress components σ_r and $\sigma_{r\phi}$ were not considered in the comparison, since they are set to zero by the boundary condition prescribed on Γ_h (2.8c). The displacement curves obtained by the semi-analytical method, and by finite elements for some values of L, are presented separately for each displacement component in Fig. 5, where the horizontal axis corresponds to the angle ϕ. The stress curves for σ_ϕ and σ_θ are given in analogous way in Fig. 6. It is noticed from Figs. 5 and 6 that, as expected, the solution obtained by the semi-analytical method is better approximated by the solution computed numerically as the value of L increases. This behaviour is seen in the displacement as well as the stress curves, being more evident in the latter case. It is also observed from Fig. 5 that the component u_r obtained semi-analytically is better approximated than the component u_ϕ obtained in the same way as the value of L increases. This difference between both displacement components can be explained by the error introduced in the numerical solution by the artificial boundary conditions, particularly on the right boundary of Ω_{tr}, which affects more strongly the displacement u_ϕ near the infinite plane surface. In order to further verify the already observed tendency as L increases, the relative error of the semi-analytical solution with respect to the numerical one was evaluated on Γ_h, for all the assumed values of L, considering separately the errors associated with the displacement vector $\boldsymbol{u}$ and the stress tensor $\boldsymbol{\sigma}(\boldsymbol{u})$. Both relative error curves as functions of L are presented in a semilogarithmic plot in Fig. 7. These curves confirm the behaviour seen in Figs. 5 and 6: The relative error between the semi-analytical and the numerical solution decreases as L increases, both for the displacement vector and the stress tensor. In fact, both relative errors show a similar tendency, being

https://doi.org/10.4208/aamm.2014.m544 Published online by Cambridge University Press

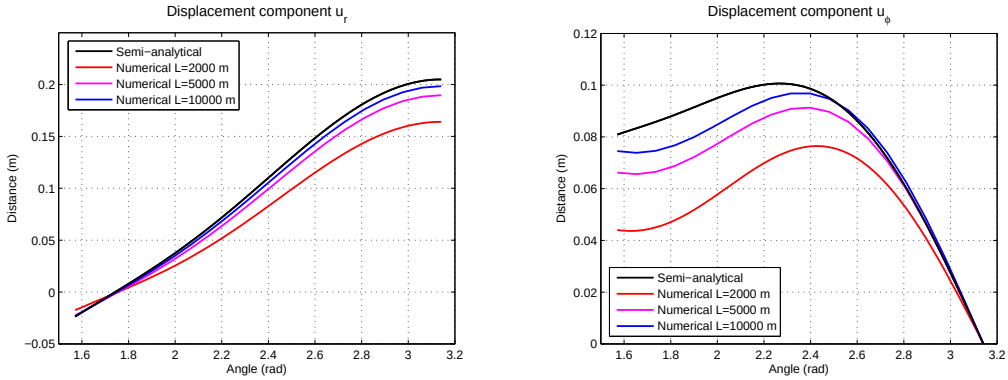


Figure 5: Comparison of displacement components on Γ_h.

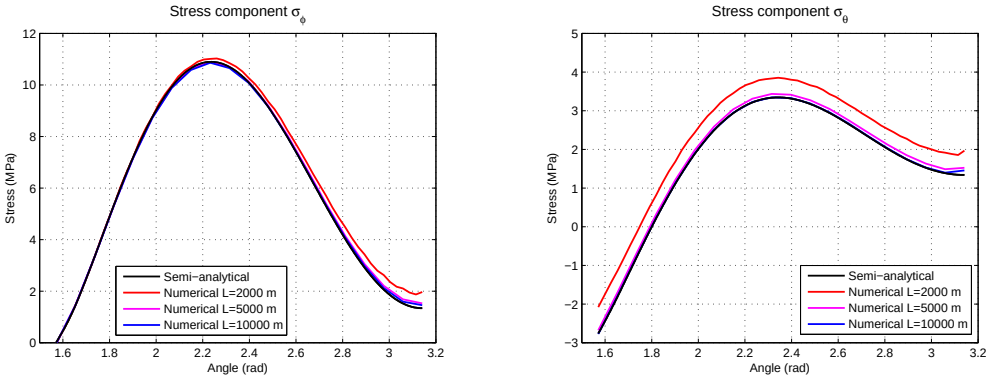


Figure 6: Comparison of stress components on Γ_h.

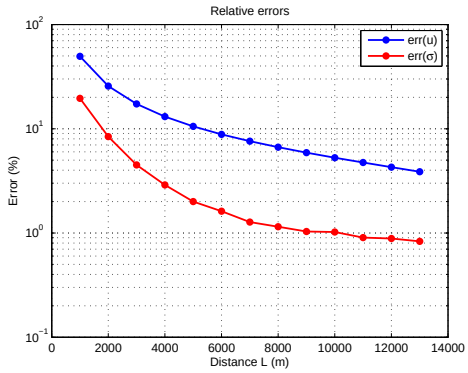


Figure 7: Relative errors associated with the displacement vector and the stress tensor on Γ_h.

the error in stress smaller than the error in displacement for all values of L. We confirm from this analysis the validity of the proposed semi-analytical solution.

https://doi.org/10.4208/aamm.2014.m544 Published online by Cambridge University Press

Appendix: Some properties of Legendre polynomials

The Legendre polynomial $P_n(\cos\phi)$ as a function of ϕ is a solution of the Legendre's differential equation, given by

$$\frac{1}{\sin\phi}\frac{\mathrm{d}}{\mathrm{d}\phi}\left(\sin\phi\frac{\mathrm{d}}{\mathrm{d}\phi}P_n(\cos\phi)\right)+n(n+1)P_n(\cos\phi)=0. \tag{A.3}$$

Some useful recurrence relations fulfilled by the Legendre polynomials and their derivatives are (cf. [2, 4]):

$$(n+1)P_{n+1}(\cos\phi)-(2n+1)\cos\phi P_n(\cos\phi)+nP_{n-1}(\cos\phi)=0, \tag{A.4a}$$
$$P'_{n+1}(\cos\phi)-P'_{n-1}(\cos\phi)=(2n+1)P_n(\cos\phi), \tag{A.4b}$$
$$\sin^2\phi P'_n(\cos\phi)=(n+1)\big(\cos\phi P_n(\cos\phi)-P_{n+1}(\cos\phi)\big), \tag{A.4c}$$
$$\sin^2\phi P'_n(\cos\phi)=n\big(P_{n-1}(\cos\phi)-\cos\phi P_n(\cos\phi)\big), \tag{A.4d}$$

where $n\geq 1$. The Legendre polynomials also satisfy the following properties for $n\geq 0$:

$$P_{2n}(0)=\frac{(-1)^n(2n)!}{2^{2n}(n!)^2}, \tag{A.5a}$$
$$P_{2n+1}(0)=0, \tag{A.5b}$$
$$P_{2n+2}(0)=-\frac{2n+1}{2n+2}P_{2n}(0), \tag{A.5c}$$
$$P'_{2n}(0)=0, \tag{A.5d}$$
$$P'_{2n+1}(0)=(2n+1)P_{2n}(0). \tag{A.5e}$$

Properties (A.5a) and (A.5b) are standard and can be found, for instance, in [2] or [4]. Property (A.5c) is a consequence of formula (A.4a). Property (A.5d) follows from (A.4c) and (A.5b). Property (A.5e) is obtained from (A.4d). Moreover, the Legendre polynomials fulfil the following integral formulae for $n\geq 0$ and $k\geq 0$:

$$\int_{\pi/2}^{\pi}P_{2n}(\cos\phi)P_{2k}(\cos\phi)\sin\phi\mathrm{d}\phi=\frac{\delta_{n,k}}{4n+1}, \tag{A.6a}$$
$$\int_{\pi/2}^{\pi}P_{2n+1}(\cos\phi)P_{2k+1}(\cos\phi)\sin\phi\mathrm{d}\phi=\frac{\delta_{n,k}}{4n+3}, \tag{A.6b}$$
$$\int_{\pi/2}^{\pi}P_{2n}(\cos\phi)P_{2k+1}(\cos\phi)\sin\phi\mathrm{d}\phi=-\frac{(2k+1)P_{2n}(0)P_{2k}(0)}{(2k+1-2n)(2k+2+2n)}, \tag{A.6c}$$
$$\int_{\pi/2}^{\pi}P'_{2n}(\cos\phi)P'_{2k}(\cos\phi)\sin^3\phi\mathrm{d}\phi=\frac{2n(2n+1)\delta_{n,k}}{4n+1}, \tag{A.6d}$$
$$\int_{\pi/2}^{\pi}P'_{2n+1}(\cos\phi)P'_{2k+1}(\cos\phi)\sin^3\phi\mathrm{d}\phi=\frac{(2n+1)(2n+2)\delta_{n,k}}{4n+3}, \tag{A.6e}$$
$$\int_{\pi/2}^{\pi}P'_{2n}(\cos\phi)P'_{2k+1}(\cos\phi)\sin^3\phi\mathrm{d}\phi=-\frac{2n(2n+1)(2k+1)P_{2n}(0)P_{2k}(0)}{(2k+1-2n)(2k+2+2n)}. \tag{A.6f}$$

https://doi.org/10.4208/aamm.2014.m544 Published online by Cambridge University Press

Formulae (A.6a), (A.6b), and (A.6c) can be deduced from [12], Subsection 7.221. To obtain (A.6c) it is, in addition, necessary to combine with (A.5a). Formulae (A.6d), (A.6e), and (A.6f) follow from formulae (A.6a), (A.6b), and (A.6c), respectively, together with the Legendre's differential equation (A.3). The following two additional integral formulae are also valid

$$\int_{\pi/2}^{\pi} P'_{2n}(\cos\phi)(1+\cos\phi)\sin\phi \mathrm{d}\phi = P_{2n}(0), \tag{A.7a}$$

$$\int_{\pi/2}^{\pi} P'_{2n+1}(\cos\phi)(1+\cos\phi)\sin\phi \mathrm{d}\phi = \frac{P_{2n}(0)}{2n+2}, \tag{A.7b}$$

which are obtained by integrating by parts and combining with (A.6a) and (A.6c), respectively.

Acknowledgments

The first author thanks the programme MECE Educación superior (2) PUC0710. The second author thanks the programmes Advanced Human Capital Job Insertion in the Industry CONICYT and Proyecto CYTED-RED Temática MAVS P711RT0278. The authors also thank Professor J.-C. Nédélec for his valuable support of this work.

References

[1] YU. A. AMENZADE, Theory of Elasticity, Mir Publishers, Moscow, 1979.
[2] L. C. ANDREWS, Special Functions for Engineers and Applied Mathematicians, Macmillan Publishing Co., New York, 1985.
[3] G. B ARFKEN AND H. J WEBER, Mathematical Methods for Physicists, Harcourt/Academic Press, London, 2001.
[4] W. W. BELL, Special Functions for Scientists and Engineers, Van Nostrand, London, 1968.
[5] Å. BJÖRCK, Numerical Methods for Least Square Problems, SIAM, Philadelphia, 1996.
[6] R. A. EUBANKS, *Stress concentration due to a hemispherical pit at a free surface*, J. Appl. Mech., 21 (1954), pp. 57–62.
[7] T. FUJITA, T. SADAYASU, E. TSUCHIDA AND I. NAKAHARA, *Stress concentration due to a hemispherical pit at a free surface of a thick plate under all-around tension*, Bull. Japan Soc. Mech. Eng., 21 (1978), pp. 561–565.
[8] T. FUJITA, E. TSUCHIDA AND I. NAKAHARA, *Asymmetric problem of a semi-infinite body having a hemispherical pit under uniaxial tension*, J. Elasticity, 12 (1982), pp. 177–192.
[9] D. GIVOLI AND J. KELLER, *A finite element method for large domains*, Comput. Methods Appl. Mech. Eng., 76 (1989), pp. 41–66.
[10] D. GIVOLI AND S. VIGDERGAUZ, *Artificial boundary conditions for 2D problems in geophysics*, Comput. Methods Appl. Mech. Eng., 110 (1993) pp. 87–101.
[11] G. H. GOLUB AND C. F. VAN LOAN, Matrix Computations, 3rd Edition, Johns Hopkins University Press, Baltimore, 1996.
[12] I. S. GRADSHTEYN AND I. M. RYZHIK, Table of Integrals, Series and Products, 7th Edition, Elsevier/Academic Press, Amsterdam, 2007.

https://doi.org/10.4208/aamm.2014.m544 Published online by Cambridge University Press

[13] H. HAN AND X. WU *Approximations of infinite boundary conditions and its application to finite elements methods*, J. Comput. Math., 3 (1985), pp. 179–192.
[14] H. HAN AND X. WU, *The approximation of the exact boundary conditions at an artificial boundary for linear elastic equations and its application*, Math. Comput., 59 (1992), pp. 21–37.
[15] M. H. SADD, Elasticity: Theory, Applications, and Numerics, Elsevier Butterworth-Heinemann, Boston, 2005.
[16] T. R. STACEY AND C. H. PAGE, Practical Handbook for Underground Rock Mechanics, Trans Tech Publications, 1986.
[17] D. L. TURCOTTE AND G. SCHUBERT, Geodynamics, Cambridge University Press, New York, 2002.
[18] A. VERRUIJT, *A complex variable solution for a deforming circular tunnel in an elastic half-plane*, Int. J. Numer. Anal. Met., 21 (1997), pp. 77–89.
[19] A. VERRUIJT, *Deformations of an elastic half-plane with a circular cavity*, Int. J. Solids Struct., 21 (1998), pp. 2795–2804.

https://doi.org/10.4208/aamm.2014.m544 Published online by Cambridge University Press